Molecular Crystals and Liquid Crystals
Publication details, including instructions for authors and subscription information:
http://www.informaworld.com/smpp/title~content=t713644168

Design, Synthesis and Characterization of Hydrogen-Bonded Ferroelectric Liquid Crystals

V. N. Vijayakumar[a]; M. L. N. Madhu Mohan[a]
[a] Liquid Crystal Research Laboratory, Bannari Amman Institute of Technology, Sathyamangalam, India

First published on: 08 July 2010

To cite this Article Vijayakumar, V. N. and Mohan, M. L. N. Madhu(2010) 'Design, Synthesis and Characterization of Hydrogen-Bonded Ferroelectric Liquid Crystals', Molecular Crystals and Liquid Crystals, 524: 1, 54 — 67
To link to this Article: DOI: 10.1080/15421406.2010.484610
URL: http://dx.doi.org/10.1080/15421406.2010.484610

Mol. Cryst. Liq. Cryst., Vol. 524: pp. 54–67, 2010

ISSN: 1542-1406 print/1563-5287 online
DOI: 10.1080/15421406.2010.484610

Taylor & Francis
Taylor & Francis Group

Design, Synthesis and Characterization of Hydrogen-Bonded Ferroelectric Liquid Crystals

V. N. VIJAYAKUMAR AND
M. L. N. MADHU MOHAN

Liquid Crystal Research Laboratory, Bannari Amman Institute of Technology, Sathyamangalam, India

*A novel series of hydrogen-bonded ferroelectric liquid crystals has been isolated. A hydrogen bond was formed between chiral ingredient (*S*)-(+)-6-methoxy-α-methyl-2-naphthaleneacetic acid (Nap) and mesogenic p-n alkyloxy benzoic acids. A phase diagram was constructed from the transition temperatures obtained by differential scanning calorimetry (DSC) and polarizing optical microscopic (POM) studies. Thermal and dielectric properties exhibited by these complexes, namely, Nap + nBA (where* n = *6 to 11), are discussed. A phase diagram of the present hydrogen-bonded series was compared with that of the free alkyloxy benzoic acids (nBA). Nap + nBA series exhibits cholesteric, smectic C*, smectic G*, and smectic F* phases. Dielectric relaxations were studied in selected members of the homologous series that exhibits cholesteric and smectic GF* phases. Dielectric studies indicate multiple relaxation processes in the cholesteric phase and a single relaxation process in smectic G*, smectic F* phase. Activation energies calculated from the respective Cole–Cole plots are discussed.*

Keywords Chemical synthesis; dielectric response; liquid crystals; optical properties; phase transitions

Introduction

Liquid crystals, discovered by Meyer *et al.* [1], are important ingredients of many display devices. Among various classes of liquid crystals, supramolecular arrangement or the self-assembly capability category is referred to as *hydrogen-bonded liquid crystals* (HBLCs). In recent years much work has been reported [2–14] in the literature on these materials relating to design, synthesis, and characterization aspects. Many research groups [15–18] are working on various synthesis routes and characterization techniques for making hydrogen-bonded ferroelectric liquid crystals (HBFLCs) suitable substitutes for existing systems.

HBLC materials have been known since the early 1960s [3,4]; however, in recent times [5–13,18–21] much work has been done on these complexes. A hydrogen bond enables various mesogenic and nonmesogenic compounds to form complexes that

Address correspondence to M. L. N. Madhu Mohan, Liquid Crystal Research Laboratory, Bannari Amman Institute of Technology, Sathyamangalam 638 401, India. E-mail: mln.madhu@gmail.com

exhibit rich phase polymorphism. HBFLCs usually are composed of a proton donor and acceptor molecules. The reported data [5–12,18–22] indicate that if an HBLC material is mesogenic it is either one of proton donor or an acceptor molecules exhibits mesogenic property. The chemical molecular structure [10,18–22] of HBFLC is co-related to the physical properties exhibited by it. The reported literature suggests the formation of HBFLC through carboxylic acids as well as from mixtures of unlike molecules capable of interacting through H-bonding [13–21]. Usually in all these HBLCs the rigid core is made up of covalent and noncovalent hydrogen bonds.

With our previous experience [23–30] in designing, synthesizing, and characterizing various types of liquid crystals, a successful attempt has been made in characterizing a novel series of inter-hydrogen-bonded ferroelectric liquid crystals.

In the present communication a homologous series of HBFLC is designed in such a way that the molecule possesses a chiral center and the hydrogen bonding is formed between the ferroelectric ingredient (*S*)-(+)-6-methoxy-α-methyl-2-naphthaleneacetic acid with mesogenic p-n alkyloxy benzoic acid. Thermal and electrical characterization of these HFBLC complexes of the present series are discussed in detail.

Experimental

Optical textural observations are made with a Nikon polarizing microscope equipped with a Nikon digital CCD camera system (Tokyo, Japan) with 5 mega pixels and $2560 * 1920$ pixel resolutions. The liquid crystalline textures are processed, analyzed, and stored with the aid of an ACT-2U imaging software system. The temperature of the liquid-crystal cell is controlled by an Instec HCS402-STC 200 temperature controller Instec (Boulder, CO, USA) to a temperature resolution of $\pm 0.1^{\circ}$C. This unit is interfaced to a computer by IEEE-STC 200 to control and monitor the temperature by the software program Wintemp. The liquid-crystal sample is filled by capillary action in its isotropic state into a commercially available (Instec) polyamide buffed cell with 4 μm spacer. Silver wires are drawn as leads from the cell. An HP 4192A LF impedance analyzer is used for dielectric studies. The transition temperatures and corresponding enthalpy values are obtained by differential scanning calorimetry (DSC), (Shimadzu DSC-60). Fourier transform infrared (FTIR) spectra are recorded (ABB FTIR MB3000) and analyzed with the MB3000 software. The p-n-alkyloxybenzoic acids (nBA) and (*S*)-(+)-6-methoxy-α-methyl-2-naphthaleneacetic acid are supplied by Sigma Aldrich (Seelze, Germany) and all the solvents used were E. Merck grade.

Synthesis of HBFLC

Intermolecular hydrogen-bonded ferroelectric mesogens are synthesized by the addition of one mole of p-n-alkyloxybenzoic acids (nBA, where $n = 6$ to 11) with one mole of (*S*)-(+)-6-methoxy-α-methyl-2-naphthaleneacetic acid (Nap) in N,N-dimethyl formamide (DMF). Further, they are subject to constant stirring for 12 h at ambient temperature of 30°C until a white precipitate in a dense solution is formed. The white crystalline crude complexes so obtained by removing excess DMF are then recrystallized with dimethyl sulfoxide (DMSO) and the yield varied from 85 to 95%. The molecular structure of the present homologous series of p-n-alkyloxybenzoic acids with (*S*)-(+)-6-methoxy-α-methyl-2-naphthaleneacetic acid is depicted in Fig. 1, where *n* represents the alkyloxy carbon number.

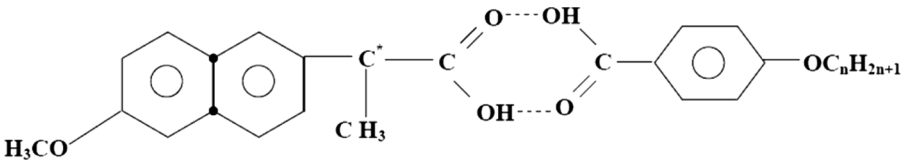

Figure 1. Molecular structure of Nap + nBA homologous series.

Results and Discussion

All the mesogens isolated under the present investigation are white crystalline solids and are stable at room temperature (30°C). They are insoluble in water and sparingly soluble in common organic solvents such as methanol, ethanol, benzene, and dichloro methane. However, they show a high degree of solubility in coordinating solvents like DMSO, DMF and pyridine. All these mesogens under present investigation melt at specific temperatures below 134°C (Table 1). They show high thermal and chemical stability when subjected to repeated thermal scans performed during polarizing optical microscopic (POM) and DSC studies.

Infrared Spectroscopy (FTIR)

IR spectra of free p-n-alkyloxybenzoic acid, Nap, and their intermolecular H-bonded ferroelectric complexes (Nap + nBA) are recorded in the solid state (KBr) at room temperature. Figure 2 illustrates the FTIR spectra of the hydrogen-bonded complex of Nap + 10BA in solid state at room temperature as a representative case. The solid-state spectra of free alkyloxybenzoic acid is reported [21] to have two sharp bands at 1685 and 1695 cm^{-1} due to the frequency ν(C=O) mode. The doubling feature of this stretching mode confirms the dimeric nature of alkyloxybenzoic acid at room temperature [21].

Further, in the present Nap + 10BA hydrogen-bonded complex, a band appearing at 2924 cm^{-1} is assigned to ν(O-H) mode of the carboxylic acid group. Furthermore, a band appearing at 1072 cm^{-1} is assigned to fundamental skeletal mode of carboxylic acid. Bands observed at 900 and 1260 cm^{-1} are assigned to ν(O-H) out-of-plane bending mode and in-plane bending of carboxylic acid, respectively. The ν(C-O) stretching in carboxylic acid is observed at 1174 cm^{-1}. A band appearing at 2550 cm^{-1} is assigned to ν(C=O) relating to the conjugate chelation mode of the intramolecular hydrogen bond.

The doubling nature of ν(C=O) mode may be attributed to the dimeric nature of the acid group at room temperature [21]. Corresponding spectrum of solution state (chloroform) shows a strong intense band, suggesting the existence of monomeric form of benzoic acid. A noteworthy feature in the spectra of Nap + 10BA complex is the appearance of a broad band at 1682 cm^{-1} and nonappearance of the doubling nature of ν(C=O) mode of benzoic acid moiety. This clearly suggests that the dimeric nature of the benzoic acid dissociates and prefers to exist in a monomeric form upon complexation.

Phase Identification

The observed phase variants, transition temperatures, and corresponding enthalpy values obtained by DSC in cooling and heating cycles for the various members of the homologous series are presented in Table 1.

Table 1. Transition temperatures in centigrade obtained by various techniques along with respective enthalpy values given in J/g

Carbon	Phase variance	Technique	Crystal to melt	Ch	C*	F*	G*	Crystal
5	No liquid crystallinity				Non mesogenic complex			
6	Ch G*	DSC (h)	105.5 (53.75)	#			#	
		DSC (c)		133.8 (1.57)			97.7 (7.27)	92.6 (28.62)
		POM (C)		134.2			98.1	92.9
7	**Ch G***	**DSC (h)**	94.7 (58.90)	105.7 (14.25)			#	
		DSC (c)		102.3 (9.34)			86.1 (21.76)	72.6 (28.70)
		POM (C)		102.8			86.5	72.9
8	Ch G*	DSC (h)	75.1 (45.21)	109.8 (17.23)			101.1 (30.63)	
		DSC (c)		103.1 (8.74)			95.1 (34.65)	50.5 (36.03)
		POM (C)		110.2			95.4	50.8
9	Ch C* G*	DSC (h)	95.4 (54.24)	109.2 (25.08)	#		#	
		DSC (c)		101.6 (7.4)	95.8 (0.37)		89.0 (17.31)	66.0 (36.93)
		POM (C)		102.0	96.2		89.3	66.2
10	Ch C* G*	DSC (h)	87.1 (30.69)	111.9 (18.65)	#		97.2 (15.25)	
		DSC (c)		111.4 (1.67)	105.0 (0.18)		91.1 (11.82)	72.6 (22.09)
		POM (C)		111.9	105.4		91.4	72.9
11	Ch C* F* G*	DSC (h)	97.6 (70.66)	#	#		#	
		DSC (c)		105.3 95.170	95.9 (6.93)	84.4 (18.22)	71.9 (13.87)	45.2 (28.41)
		POM (C)		105.8	96.4	84.9	72.3	45.5

Monotropic transition; (h) Heating run; (c) Cooling run.

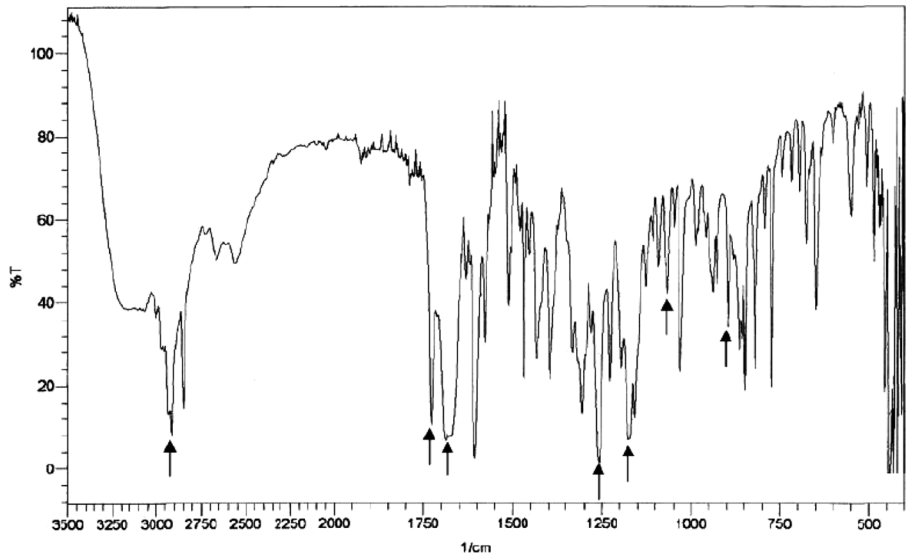

Figure 2. FTIR of Nap + 10BA complex.

Nap + nBA Homologous Series

The mesogens of the Nap and alkyloxy benzoic acid homologous series are found to exhibit characteristic textures [31–34], viz. cholesteric (droplets), smectic C* (schlieren texture), smectic F* (broken focal conic), and smectic G* (multi colored mosaic texture) respectively. The general phase sequence of the Nap with hexyloxy benzoic acid (Nap + 6BA), heptyloxy benzoic acid (Nap + 7BA), octyloxy benzoic acid (Nap + 8BA), nonyloxy benzoic acid (Nap + 9BA), decyloxy benzoic acid (Nap + 10BA), and undecyloxy benzoic acid (Nap + 11BA), respectively, in the cooling run can be shown as:

$$\text{Isotropic} \rightarrow \text{Ch} \rightarrow \text{Sm G}^* \rightarrow \text{Crystal} \qquad (\text{Nap} + 6\text{BA}, \text{Nap} + 7\text{BA}, \text{Nap} + 8\text{BA})$$

$$\text{Isotropic} \rightarrow \text{Ch} \rightarrow \text{Sm C}^* \rightarrow \text{Sm G}^* \rightarrow \text{Crystal} \qquad (\text{Nap} + 9\text{BA}), (\text{Nap} + 10\text{BA})$$

$$\text{Isotropic} \rightarrow \text{Sm C}^* \rightarrow \text{Sm F}^* \rightarrow \text{Sm G}^* \rightarrow \text{Crystal} \qquad (\text{Nap} + 11\text{BA})$$

It is noteworthy to mention that pentyloxy benzoic acid complex (Nap + 5BA) does not exhibit any liquid-crystalline property.

Paramorphic Textural Changes

As discussed above, all the complexes of Nap + nBA exhibit various phases characterized by textural observations. It is worth mentioning the paramorphic textural changes observed in smectic G*. As a representative case, smectic G* texture of Nap + 6BA is discussed. As the liquid crystal complex Nap + 6BA is cooled from cholesteric phase (133.8°C) to smectic G* phase (97.7°C) the multicolored mosaic texture is observed (Plate 1a) with bright blue stripes. As the temperature is decreased to 95.1°C, the color of the texture changes from bright blue to light green (Plate 1b). A further decrease of the temperature to 92.8°C results in the reddish

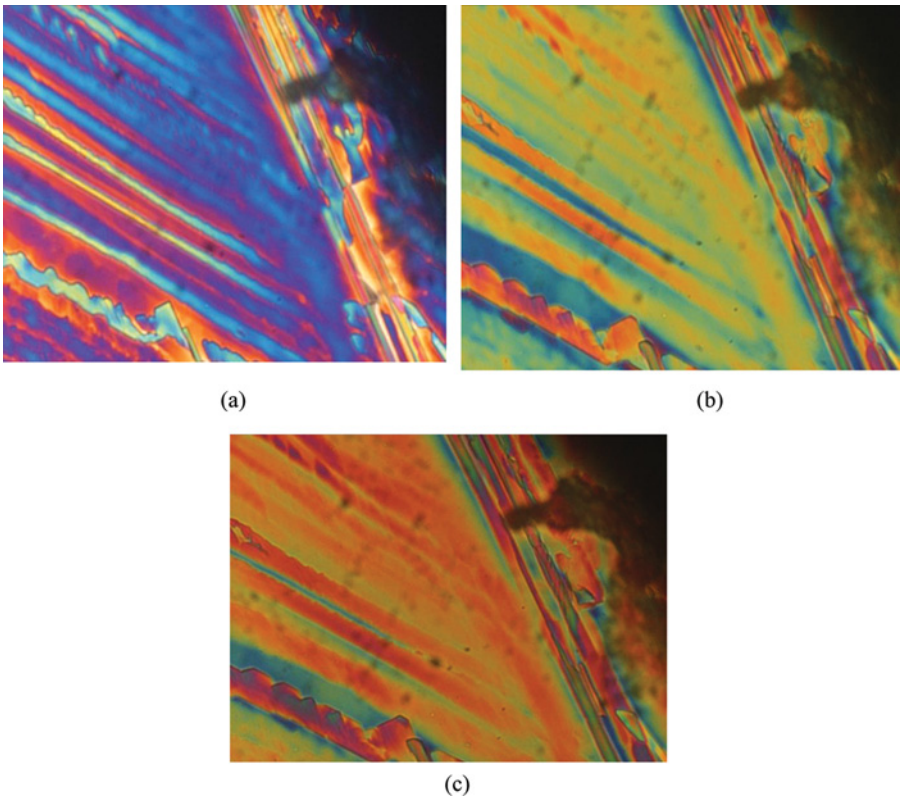

Plate 1. (a) Multicolored mosaic texture of smectic G* phase in Nap + 6BA with blue tinge observed at 97.7°C. (b) Paramorphic changes in the texture of smectic G* phase in Nap + 6BA 6BA with blue tinge observed at 95.1°C. (c) Paramorphic changes in the texture of smectic G* phase in Nap + 6BA with blue tinge observed at 92.8°C.

color of the texture (Plate 1c). It is important to note that the texture of the smectic G* phase is unaltered but the color of the texture is changed. These paramorphic changes in the texture of smectic G* are attributed to the change in the birefringence of the material with the temperature.

DSC Studies

DSC thermograms are obtained in heating and cooling cycles. The sample is heated with a scan rate of 10°C/min and held at its isotropic temperature for one minute to attain thermal stability. The cooling run is also performed with a scan rate of 10°C/min. The respective equilibrium transition temperatures and corresponding enthalpy values of the mesogens of the homologous series are listed separately in Table 1. In the DSC heating run, smectic G* phase of Nap + 6BA, Nap + 7BA, Nap + 9BA, and Nap + 11BA are observed to be monotropic transitions, whereas smectic C* is observed to be monotropic transition in Nap + 9BA, Nap + 10BA, and Nap + 11BA and cholesteric phase is observed to be monotropic in Nap + 6BA and Nap + 11BA complexes, respectively. All other transitions are classified as enantiotropic transitions. Polarizing optical microscopic studies are concurrent with the DSC results.

DSC Studies of Nap + 10BA

As a representative case, the phase transition temperatures and enthalpy values of Nap + 10BA complex are discussed. Figure 3 illustrates the thermogram of Nap + 10BA hydrogen-bonded complex recorded at a scan rate of 10°C/min for the heating and cooling runs, respectively. In the cooling run of the DSC thermogram the above compound possesses four distinct transitions, namely, isotropic to cholesteric, cholesteric to Sm C*, Sm C* to Sm G*, and Sm G* to crystal with transition temperatures of 111.4°C, 105.0°C, 91.1°C, 72.6°C, and with corresponding enthalpy values of 1.67, 0.18, 11.82, 22.09 J/g, respectively. In the heating cycle three distinct transitions namely, crystal to melt, melt to cholesteric, and cholesteric to Sm G*, are obtained at 87.1°C, 111.9°C, 97.2°C, with corresponding enthalpy values of 30.69, 18.65, 15.25 J/g, respectively. All these transition temperatures of the present homologous series concur with POM studies.

Phase Diagram of Pure p-n-Alkyloxybenzoic Acids

The phase diagrams of pure p-n-alkyloxybenzoic acids (Fig. 4) were reported by us [24] and the Nap + nBA homologous series is constructed through optical polarizing microscopic studies and by the phase transition temperatures observed in the cooling run of the DSC thermogram. The phase diagram of pure p-n-alkyloxybenzoic acid is composed of three phases, namely, nematic, smectic C, and smectic G.

Phase Diagram of Nap + nBA Homologous Series

The phase diagram of Nap + nBA complexes is depicted in Fig. 5. A careful observation of Fig. 4 reveals the following points:

a. Four phases, namely, cholesteric, and smectic C*, G*, and F*, have been observed in the phase diagram.
b. Two phases, namely, cholesteric and smectic G*, are observed in all the members of the homologous series; further, it can be noticed that the former phase

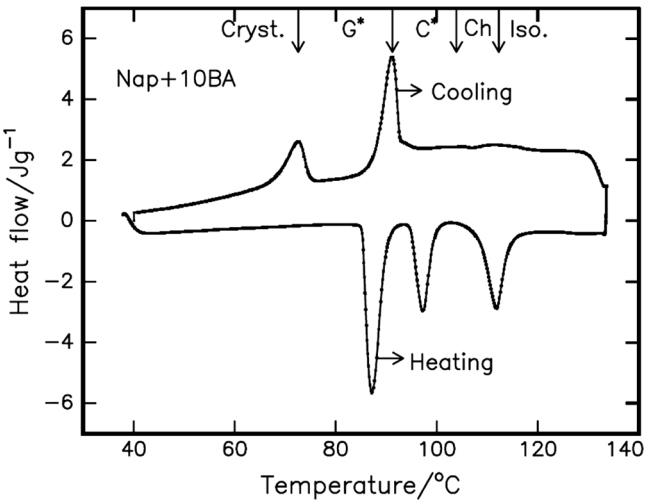

Figure 3. DSC thermogram of Nap + 10BA complex.

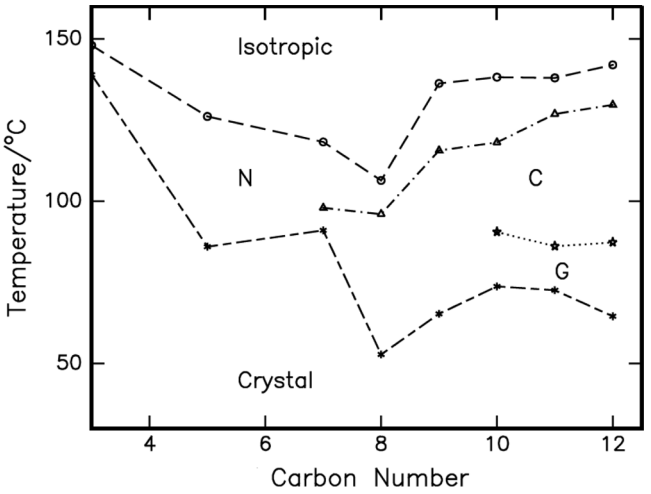

Figure 4. Phase diagram of pure alkoxy benzoic (nBA) acids.

(cholesteric) is the initial phase, whereas the latter phase (smectic G*) appeared as the last phase in the entire series.

c. At every increment of the odd alkoxy carbon number a new phase has been induced. As an example, smectic C* phase has been observed from nonyloxy complex (Nap + 9BA) and smectic F* has been induced at undecyloxy complex (Nap + 11BA).
d. The thermal range of smectic G* phase is observed to be twofold that of the thermal range of cholesteric phase in the Nap + nBA phase diagram.
e. The mesogenic thermal range of the homologous series gradually increased with the increment in the alkyloxy carbon number.
f. In the present HBFLC series, odd–even effect has a pronounced influence on the cholesteric to smectic G* transition temperatures; in other words, all the even

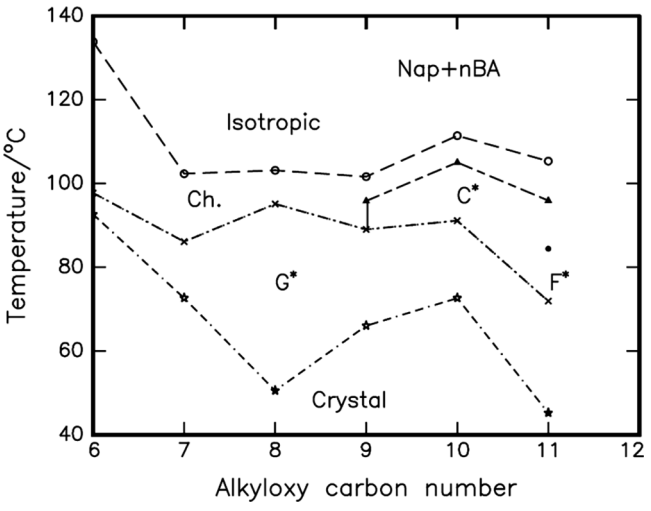

Figure 5. Phase diagram of Nap + nBA homologous series.

complexes follow one pattern and the odd complexes follow yet another pattern. This odd–even effect is in concurrence with the reported [35–39] literature on thermotropic liquid crystals. The odd–even effect observed at the cholesteric to smectic G* transition is pronounced compared to the smectic G* to crystal transition temperatures.

Comparision of Phase Diagrams

a. Compared to the pure alkyloxy benzoic acid phase diagram (Fig. 4), in the present hydrogen-bonded ferroelectric homologous series (Fig. 5), the thermal range of smectic G* phase has been drastically increased and it has quenched the nematic phase in the lower homologous members, and a new higher ordered smectic F* phase has been induced in the Nap + 11BA complex. The chain length and the molecular width of the HBFLC favored induction of new smectic orderings.
b. Compared to the pure benzoic acid phase diagram in the present HBFLC series the isotropic temperatures have considerably reduced, whereas the crystallization temperatures are unaltered. This may be attributed to the increased chain length and enhanced conjugation in the present HBFLC series.

Dielectric Relaxations in Smectic G* and Cholesteric Phases

Dielectric dispersion, *i.e.*, frequency variation of dielectric loss exhibited by various HBFLC compounds studied at different temperatures in cholesteric and smectic G* phases in the frequency range of 5 Hz to 13 MHz, is discussed below. An impedance analyzer (HP4192A) is operated with 1 $V_{P\text{-}P}$ oscillating signal with zero bias fields. Relative permittivity $\varepsilon'_r(\omega)$ and dielectric loss $\varepsilon''(\omega)$ are calculated by the following equations;

$$^*\varepsilon'_r(\omega) = \varepsilon'_r(\omega) - j\varepsilon''(\omega)$$

$$\varepsilon'_r(\omega) = [C_{LC} - C_{leads}]/[C_{empty} - C_{leads}]$$

$$^*\varepsilon'_r(\omega) = \text{Tan } \delta(\omega)\,^*\varepsilon_r(\omega)$$

To detect the possible relaxation in the HBFLC complexes, the mesogens are scanned in the frequency range of 5 Hz to 13 MHz at different temperatures corresponding to various phases. Two types of relaxation mechanisms, namely, multiple relaxation process and Type I relaxation are observed in the cholesteric and smectic G* phases of Nap + nBA ($n = 8, 9, 10$) mesogens respectively.

Type I Relaxation

Two types of relaxation mechanisms are observed in the present HBFLC homologous series. Type I relaxation is observed in the mesogens at higher frequencies of several megahertz. In this type of relaxation mechanism, relaxation is not suppressed by the applied bias voltage. The type I relaxations are related to the reorientation mechanism of longitudinal dipole moment to the applied field. Further, the reorientation of the longitudinal dipole moment pertaining to the flexible end chain bridged by an electronegative oxygen atom is observed to respond rather slowly to the external field in type I relaxation.

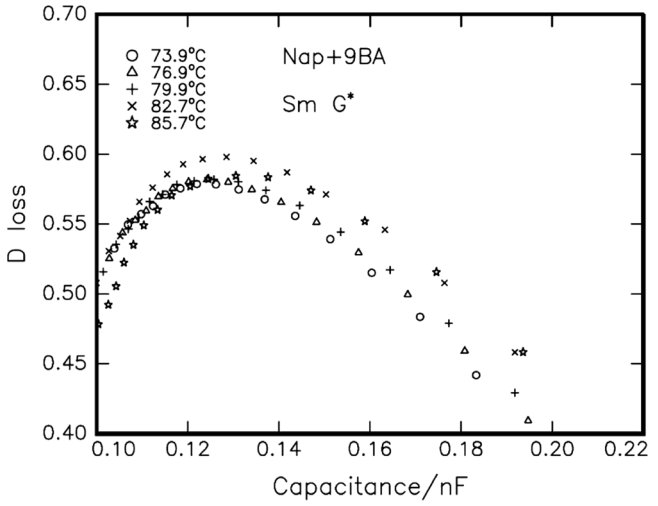

Figure 6. Cole–Cole plots in smectic G* of Nap + 9BA.

As a representative case, the Cole–Cole plots for Nap + 8BA in smectic G* phase at 73.9°C, 76.9°C, 79.9°C, 82.7°C, and 85.7°C are illustrated in Fig. 6. With increment in the temperature, the shift in the relaxation frequency is depicted as variation in the maximum value of the dielectric loss. It can seen that the relaxation exhibits a Cole–Cole type variation. It can be observed from Fig. 7 that the relaxation frequency (f_r) is inversely proportional to the temperature (smectic G* to crystal). The high activation energy possessed by these systems is in agreement with that reported in the literature [40–46].

Figure 7 illustrates the Arrhenius plots for Nap + 8BA, Nap + 9BA, and Nap + 10BA complexes in the smectic G* phase. One can notice that the slope of

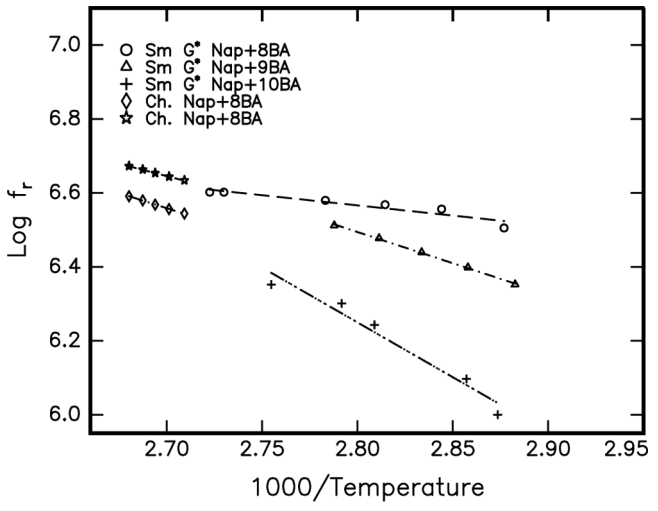

Figure 7. Arrhenius plots for various relaxation processes in Nap + nBA series.

Table 2. Relaxation frequencies and corresponding activation energies

HBFLC complex	Phase	Type	Relaxation frequency (f_r) (MHz)	Activation energy (eV)
Nap + 8BA	G*	Type I	3.80	0.097
	Ch.	Type II	3.70	0.038
	Ch.		4.50	0.346
Nap + 9BA	G*	Type I	2.75	0.023
Nap + 10BA	G*	Type I	1.75	0.020

these curves gradually increases with the increment in the alkyloxy carbon number. Thus, the chain length has a pivotal influence on the activation energies possessed by the individual HBFLC. These values of the activation energies are listed in Table 2.

Type II Relaxation

In addition to the above relaxation mode another type of relaxation, called type II relaxation (multiple relaxations), has been investigated.

As a representative case the Cole–Cole plots for Nap + 8BA complex in cholesteric phase at 93.1°C, 94.2°C, 96.2°C, 98.1°C, and 100.1°C are shown in Fig. 8. The relevant activation energies for both the relaxation processes are given Table 2. It can be observed from Fig. 8 that the relaxation frequency (f_r) is inversely proportional to the temperature (cholesteric to smectic G*). Transverse dipoles originate this type of relaxation. The contribution of these dipoles is comparatively low to the longitudinal counterparts. The hydrogen bonding and its flexible moiety also contribute to this type of relaxation. The low activation energies of this type of relaxation are expected and are in concurrence with reported [40–46] literature

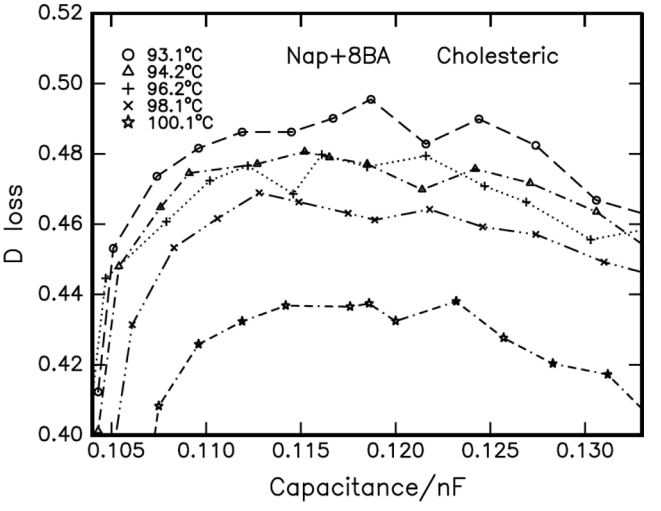

Figure 8. Cole–Cole plots in cholesteric phase of Nap + 9BA.

values. The multiple relaxation phenomena indicate that the bridging group in the central core part of liquid-crystal moiety is more rigidly fixed in the molecular structure than the end chains, which are relatively free to rotate.

Molecular Modeling

The distinct response of the dipolar orientations evinced experimentally in the present hydrogen-bonded ferroelectric Nap + nBA series as type I and type II (multiple relaxations in cholesteric phase) are attributed to the molecular modeling illustrated in Fig. 9. The assignment of type I and type II relaxations is argued in the proposed model (Fig. 9) as follows:

a. The molecular structure is made up of rigid core composed of biphenyl rings.
b. The flexible moiety includes the hydrogen bonding and the alkyloxy benzoic acid chain length.
c. Furthermore, one can notice a good number of longitudinal dipoles (μ_L) aligning parallel to the molecular structure.
d. Transverse dipoles (μ_T) align perpendicular to the molecular structure.

The type I relaxation mechanism is attributed to the longitudinal dipole moment (μ_l) situated at the corner of the rigid part of the molecule. In the present series this longitudinal dipole moment (μ_L) is observed as the oxygen molecule attached to the side of the benzene core structure of HBFLC. These longitudinal dipoles enhance the conjugation and in turn the strong dipolar correlation is achieved, which is thus responsible for the type I relaxation with high activation energy. In addition to these longitudinal dipoles, type I relaxation is attributed to the rigid core comprising the biphenyl rings.

The multiple relaxation mechanism is attributed to the transverse dipole moment (μ_T) situated at the flexible part of the molecular structure at the chiral carbon of HBFLC mesogen. The contribution of the laterally substituted dipoles is rather small, which can be evinced through the magnitude of the corresponding activation energy. The flexible moieties of the mesogen also contribute to the multiple relaxations phenomenon.

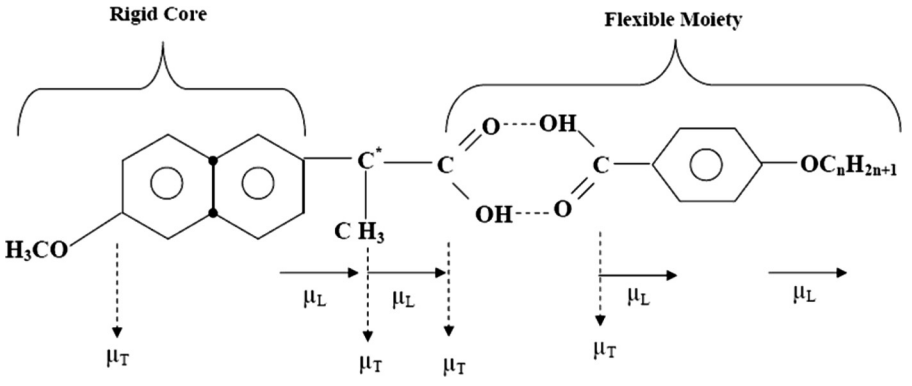

Figure 9. Molecular modeling for various relaxation processes.

Conclusions

An inter-hydrogen-bonded liquid-crystalline complex between alkoxy benzoic acid (nBA) and methoxy-α-methyl-2-naphthaleneacetic acid (Nap) has been successfully isolated and characterized. Smectic G^* phase is observed to be induced in the lower homologous series of the complex and smectic F^* are observed in the higher homologous series. DSC, dielectric, and textural studies confirm the above observations. Single and multiple relaxations are detected in smectic G^* and cholesteric phases, respectively.

Acknowledgments

The authors acknowledge the financial support rendered by All India Council of Technical Education, Department of Science and Technology, and Defence Research Development Organization, New Delhi. Infrastructural support provided by Bannari Amman Institute of Technology is gratefully acknowledged.

References

[1] Meyer, R. B., Liebert, L., Strezelecki, L., & Keller, P. (1975). *J. Physique. Lett.*, *30*, 69.
[2] Kato, T. (1998). *Handbook of Liquid Crystals*, Wiley-VCH: Weinheim, Germany.
[3] Gray, G. W. (1962). *Molecular Structure and Properties of Liquid Crystals*, Academic Press: London.
[4] Kelker, H., & Hatz, R. (1980). *Handbook of Liquid Crystals*, Verlag Chemie: Weinheim, Germany.
[5] Kato, T., & Frechet, J. M. J. (1993). *J. Am. Chem. Soc.*, *111*, 8533.
[6] Yu, L. (1993). *Liq. Cryst.*, *14*, 1303.
[7] Kato, T., Kihara, H., Uryu, T., Ujiie, S., Iimura, K., Fréchet, J. M. J., & Kumar, U. (1993). *Ferroelectrics*, *148*, 161.
[8] Kato, T., Uryu, T., Kaneuchi, F., Jin, C., & Fréchet, J. M. J. (1993). *Liq. Cryst.*, *14*, 1311.
[9] Demus, D., Demus, H., & Zaschke, H. (1974). *Flussige Kristalle Tabellen*, VEB Deutcher Verlag fur Grundstoffindustrie: Leipzig, Germany.
[10] Paleos, C. M., Tsiourvas, D. (2001). *Liq. Cryst.*, *28*, 1127.
[11] Xu, B., Swager, T. M. (1995). *J. Am. Chem. Soc.*, *117*, 5011.
[12] Malik, S., Dhal, P. K., & Mashelkar, R. A. (1995). *Macromolecules*, *28*, 2159.
[13] Sideratou, Z., Tsiourvas, D., Paleos, C. M., & Skoulios, A. (1997). *Liq. Cryst.*, *22*, 51.
[14] Goodby, J. W., Blinc, R., Clark, N. A., Lagerwall, S. T., Osipov, S. A., Pikin, S. A., Sakurai, T., Yoshino, Y., & Zecks, B. (1991). *Ferro Electric Liquid Crystal, Principles, Properties, and Applications*, Gordon and Breach Press: Philadalphia.
[15] Clark, N. A., & Lagerwall, S. T. (1980). *Appl. Phys. Lett.*, *36*, 899.
[16] Vijayakumar, V. N., & Madhu Mohan, M. L. N. (2009). *Solid State Commun.*, *149*, 2090.
[17] Vijayakumar, V. N., & Madhu Mohan, M. L. N. (2009). *Braz. J. Phys.*, *39*, 600.
[18] Kumar, P. A., Srinivasulu, M., & Pisipati, V. G. K. M. (1999). *Liq. Cryst.*, *26*, 859.
[19] Swathi, P., Kumar, P. A., & Pisipati, V. G. K. M. (2000). *Liq. Cryst.*, *27*, 665.
[20] Srinivasulu, M., Satyanarayana, P. V. V., Kumar, P. A., & Pisipati, V. G. K. M. (2001). *Liq. Cryst.*, *28*, 1321.
[21] Nakamoto, K. (1978). *Infrared and Raman Spectra of Inorganic and Co-ordination Compounds*, Interscience: New York.
[22] (a) Sreedevi, B., Chalapathi, P. V., Srinivasulu, M., Pisipati, V. G. K. M., & Potukuchi, D. M. (2004). *Liq. Cryst.*, *31*, 303; (b) Potukuchi, D. M., Goud, B. V. S., & Pisipati, V. G. K. M. (2002). *Ferroelectrics*, *289*, 77; (c) Sreedevi, B., Chalapathi, P. V., Kotikalapudi, V. K. M., Pisipati, V. G. K. M., & Potukuchi, D. M. (2007). *Ferroelectrics*, *361*, 18.

[23] Chitravel, T., Madhu Mohan, M. L. N., and Krishnakumar, V. (2008). *Mol. Cryst. Liq. Cryst.*, *493*, 17.
[24] Vijayakumar, V. N., Murugadass, K., & Madhu Mohan, M. L. N. (2009). *Mol. Cryst. Liq. Cryst.*, *515*, 37.
[25] (a) Madhu Mohan, M. L. N., Arunachalam, B., & Arravindh Sankar, C. (2008). *Metal. & Mater. Trans. A*, *39*, 1192; (b) Madhu Mohan, M. L. N., & Arunachalam, B. (2008). *Z. Natur. for ch.*, *63a*, 435.
[26] Madhu Mohan, M. L. N., & Pisipati, V. G. K. M. (2000). *Liq. Cryst.*, *26*, 1609.
[27] (a) Kumar, P. A., Madhu Mohan, M. L. N., & Pisipati, V. G. K. M. (2000). *Liq. Cryst.*, *27*, 1533; (b) Vijayakumar, V. N., & Madhu Mohan, M. L. N. (2009). *Braz. J. Phys.*, *39*, 4.
[28] Madhu Mohan, M. L. N., Kumar, P. A., Goud, B. V. S., & Pisipati, V. G. K. M. (1999). *Mater. Res. Bull.*, *34*, 2167.
[29] (a) Madhu Mohan, M. L. N., Kumar, P. A., & Pisipati, V. G. K. M. (1999). *Ferroelectrics*, *227*, 105; (b) Vijayakumar, V. N., Murugadoss, K., & Madhu Mohan, M. L. N. (2009). *Mol. Cryst. Liq. Cryst.*, *515*, 37.
[30] Vijayakumar, V. N., & Madhu Mohan, M. L. N. (2009). *Ferroelectrics*, *392*, 81.
[31] Gray, G. W., & Goodby, J. W. G. (1984). *Smetic Liquid Crystals—Textures and Structures*, Leonard Hill: London.
[32] Kumar, S. (2001). *Liquid Crystals: Experimental Study of Physical Properties and Phase Transitions*, Cambridge Press: Cambridge.
[33] de Gennes, P. G. (1974). *The Physics of Liquid Crystals*, Oxford Press: London.
[34] Stanley, H. E. (1971). *Introduction to Phase Transition and Critical Phenomena*, Oxford University Press, USA.
[35] Roviello, A., Sirigu, A. (2003). *Makromol. Chem.*, *183*, 895.
[36] Marcelis, A. T. M., Koudijs, A., & Sudholter, E. J. R. (1995). *Liq. Cryst.*, *18*, 851.
[37] Pines, A., Ruben, D. J., & Allison, S. (1974). *Phys. Rev. Lett.*, *33*, 1002.
[38] Kuribayashi, M., & Hori, K. (1999). *Liq. Cryst.*, *26*, 809.
[39] Craig, A. A., Imrie, C. T. (1995). *Macromol*, *28*, 3617.
[40] Padmaja Rani, G., Potukuchi, D. M., Rao, N. V. S., & Pisipati, V. G. K. M. (1994). *Solid State Comm.*, *92*, 349.
[41] Jose, P. P., & Bagchi, B. (2006). *J. Chem. Phys.*, *125*, 1.
[42] Chan, P. K. (2001). *Liq. Cryst.*, *28*, 207.
[43] Chan, P. K., Lee, K. W. D., and Tran, T. L. (2001). *Comput. Mater. Sci.*, *21*, 329.
[44] Sreedevi, B., Chalapathi, P. V., Kotikalapudi, V. K. M., Pisipati, V. G. K. M., & Potukuchi, D. M. (2009). *Mol. Cryst. Liq. Cryst.*, *515*, 69.
[45] Padmaja Rani, G., Potukuchi, D. M., & Pisipati, V. G. K. M. (1998). *Liq. Cryst.*, *25*, 589.
[46] Kress, H., Tschierske, S., Hohmuth, A., Stotzer, C., & Weissflog, W. (1996). *Liq. Cryst.*, *20*, 715.